Orbit Ephemeris Monitors for Local Area Differential GPS

BORIS PERVAN
LIVIO GRATTON
Illinois Institute of Technology

Methodologies sufficient to monitor GPS satellite orbit ephemeris for Category I aircraft precision approach navigation are described. In the absence of a satellite maneuver, it is shown that a monitor based on the projection of previously validated ephemeris parameters is adequate to meet navigation integrity and availability requirements. After scheduled stationkeeping maneuvers, no previously validated ephemerides are available, so a measurement-based method is required. The feasibility of such a monitor is also established.

Manuscript received October 14, 2003; revised October 3 and November 21, 2004; released for publication November 21, 2004.

IEEE Log No. T-AES/41/2/849011.

Refereeing of this contribution was handled by J. L. Leva.

This work was supported by the Federal Aviation Administration.

Authors' address: Dept. of Mechanical Materials and Aerospace Engineering, Illinois Institute of Technology, Engineering I Bldg., 10 West 23rd St., Chicago, IL 60616-3793, E-mail: (Pervan@iit.edu).

I. INTRODUCTION

Each GPS space vehicle (SV) broadcasts orbit ephemerides so users can compute satellite locations at any time of interest. The satellite locations, together with ranging measurements obtained from the SV signals, are used to compute user position. An error in the knowledge of satellite position will therefore cause a resulting error in this computation.

Differential GPS (DGPS) is a powerful means of eliminating many error sources. Knowing the exact location of a ground antenna, and using the broadcast ephemerides, a geometric range can be computed to each satellite. The difference between the computed range and the measured range is called a DGPS ranging correction. This correction is broadcasted to local DGPS users to eliminate errors common to the user and reference. However, some errors that are common over short user-reference displacements tend to decorrelate as the displacement increases. For example, since the DGPS corrections are derived from scalar ranges, satellite position error components orthogonal to the satellite line-of-sight (LOS) direction are not accounted for. As the user-reference distance becomes larger, such a satellite position error will manifest itself as a differential ranging error.

Currently, the FAA is transitioning the National Airspace System (NAS) from ground-based to satellite-based navigational aids. The new NAS architecture would consist of GPS, the wide area augmentation system (WAAS), and the local area augmentation system (LAAS). LAAS is intended to be the primary radio-navigation system for Category I, II, and III precision approach and landing. The Category I system is a single frequency LAAS architecture that will be implemented first, and it is the object of this work.

A distinguishing feature of LAAS, when compared with other DGPS implementations, is that it uses multiple receivers with high performance multipath limiting antennas (MLA). The use of multiple MLA antennas in LAAS is motivated by the stringent requirements on navigation accuracy, integrity, continuity, and availability. Redundancy in reference receiver implementation and antenna spatial separation are particularly advantageous from an integrity perspective because they provide means for fault detection, including the detection of orbit ephemeris anomalies. To ensure integrity, the LAAS navigation system must reliably detect failures and anomalies that lead to hazardously misleading information at the aircraft. The work presented here describes sufficient methodologies to monitor GPS satellite orbit ephemeris for Category I LAAS.

Two basic types of orbit ephemeris threat are recognized, the first type being subdivided into two separate classes.

Type A: The broadcast ephemeris data is erroneous following a satellite maneuver.

Type A1: The occurrence of the satellite maneuver is known to the LAAS Ground Facility (LGF).

Type A2: The LGF is unaware of the satellite maneuver.

Type B: The broadcast ephemeris data is erroneous, but no satellite maneuvers are involved.

Both type A and type B events can cause differential ranging errors. However, the ramifications of these failure classes differ in both likelihood of occurrence and means of detection. The likelihood of type B failures is relatively higher than type A because orbit ephemeris uploads and broadcast ephemeris changeovers are frequent (nominally once per day and once every 2 h, respectively, for each satellite), whereas spacecraft maneuvers are rare (no more than once or twice per year). Unannounced or unintentional maneuvers (type A2) represent a very small subset of all spacecraft maneuvers. They are not considered as credible for LAAS Category I and are therefore not covered in this paper. (Type A2 events will be addressed in the future for Category II/III applications.)

With regard to means of detection, type B failures are easier to detect than type A1 because anomalies of the former type can be identified by comparison with prior validated broadcast ephemerides. In contrast, prior ephemerides are of no use in the detection of type A1 failures because of the intervening maneuver. Ideally, the monitors to be implemented should be able to detect both types of failures. Because the ephemeris messages for each satellite are created and broadcasted independently, and ephemeris anomalies are low probability events, the likelihood of multiple simultaneous ephemeris failures is assumed to be negligible. Thus for the work described here, the maximum number of satellites with ephemeris failures at any time is assumed to be one.

LAAS specifications assign the responsibility for detecting significant ephemeris discrepancies to the LGF, rather than to the users. However, it is recognized that any monitor implementation, LGF or aircraft-based, will be imperfect (i.e., smaller ephemeris errors will be difficult to detect) and any undetected orbit error will ultimately cause navigation errors that are dependent on the (time-varying) aircraft/LGF displacement. Therefore, the impact of possible undetected orbit errors on navigation must ultimately be assessed separately by each individual aircraft within the LAAS service volume. Accordingly, along with the DGPS ranging correction, the LGF will also broadcast information regarding the minimum ephemeris error detectable by the ephemeris monitor. The aircraft uses this information to compute protection levels under the hypothesis of an ephemeris failure. The protection level is a position domain bound on navigation error that is consistent with the allowable integrity risk. An alarm condition will be triggered at the aircraft when a protection level exceeds a fixed alert limit established in the LAAS minimum operational performance standards (MOPS) [1]. The capability to generate such alarms is necessary to maintain navigation integrity. However, to ensure that navigation continuity and availability are not adversely affected by false alarms, it is important to ensure that the minimum detectable ephemeris error is small.

Prior work by Pervan and Chan [2] focused on the use of dual frequency measurements for real-time ephemeris anomaly detection. These results are applicable for Category II and III implementations, where dual frequency ground measurements may be available, but they are not directly relevant for Category I. Work by Pullen, et al. [3] derives the vertical protection level under the ephemeris failure hypothesis, and introduces basic concepts for Category I LAAS orbit ephemeris monitoring that are further extended in this work. These include verification of the consistency of new and old ephemeris messages for type B anomaly detection, and measurement-based detection for type A1 events. The potential use of WAAS broadcast data for ephemeris error mitigation in LAAS is not considered in this work because LAAS functionality must exist in environments where WAAS is unavailable.

II. PROTECTION LEVELS AND MINIMUM DETECTABLE ERROR

The measured pseudo-range for a given satellite at the LGF or the aircraft is

$$\rho = r + c[\delta t_u - \delta t^s] + I + T + \upsilon \tag{1}$$

where

- ρ pseudo-range measurement,
- r true user-satellite distance,
- δt_u receiver clock offset with respect to the GPS system time,
- δt^s satellite clock offset with respect to the GPS system time,
- I signal delay due to the ionosphere,
- T signal delay due to the troposphere,
- υ multipath and receiver thermal noise.

The range correction (RC) for each satellite is obtained at the LGF by subtracting an estimate of the range ($\hat{\rho}$) from the pseudo-range:

$$\mathrm{RC} = \rho_{\mathrm{LGF}} - \hat{\rho} \tag{2}$$

where $\hat{\rho}$ is obtained by computing the vector displacement from the known LGF antenna position to the satellite position derived from the broadcast ephemeris.

When the aircraft subtracts this correction from its own pseudo-range for the same satellite (ρ_{air}) the effective differential ranging error ($\Delta\rho$) remaining will be:

$$\Delta\rho = c\Delta\delta t_u + \Delta T + \Delta I + \Delta eph + \Delta\upsilon. \quad (3)$$

In (3), ΔI and ΔT represent the potentially differing effects of the ionosphere and troposphere at the LGF and aircraft. These terms are nominally very small relative to the anomalous ephemeris effects considered in this work and are not treated further here. The term $\Delta\upsilon$ represents the differential ranging error due to thermal noise and multipath, which are independent between the aircraft and reference receivers. The relative receiver clock offset $\Delta\delta t_u$ is easily estimated in the DGPS positioning process using four or more satellites. The term Δeph represents the portion of the differential ranging error caused by an error in the satellite position knowledge.

GPS satellite orbit information is transmitted by the GPS control segment to users by modulating orbit parameter data on the satellite ranging signals. A simplified orbital model of 15 parameters is used to generate satellite position, which is nominally very accurate ($\sim$ 3 m 1 σ error) [4] for a limited period of time, and is updated every 2 h. Nominally Δeph is extremely small for LAAS (less than a millimeter). However, if there is an anomalous condition in the SV ephemeris, the Δeph term may be much larger, causing a navigation hazard.

Defining x to be the vector displacement between the aircraft antenna and the geometric centroid of the LGF antennas and δe_i as the error in the LOS unit vector from the LGF to spacecraft i resulting from the use of an erroneous satellite ephemeris, it is shown in [5] that

$$\Delta eph_i = \delta e_i^{\mathrm{T}} x \quad (4)$$

and that δe_i can be expressed to first order directly as a function of the SV position error δr_i to yield

$$\Delta eph_i = \frac{\delta r_i^{\mathrm{T}}(I - e_i e_i^{\mathrm{T}})x}{\rho_i} \quad (5)$$

where ρ_i is the scalar range to the satellite i, e_i is the 3×1 LOS unit vector generated using the broadcast ephemeris, and I is the 3×3 identity matrix. This formula directly relates SV position error to differential ranging error. It is clear that the magnitude of the resulting ranging error scales linearly with both the aircraft distance from the LGF and the magnitude of the satellite position error orthogonal to the LOS.

To take into account the possibility of an error in the computed satellite position that is undetected by LGF monitoring, the aircraft is required to compute vertical and lateral protection levels under the hypothesis of an ephemeris failure (VPL_e and LPL_e). The equation corresponding to the vertical case is derived in [3] and specified in [1]:

$$\text{VPL}_e(i) = P_i|S_{\text{vert},i}||x| + k_{\text{md}}\sqrt{\sum_{j=1}^{n} S_{\text{vert},j}^2\sigma_j^2}$$

$$\Rightarrow \text{VPL}_e = \max_i \text{VPL}_e(i) \quad (6)$$

where

$S_{\text{vert},i}$, is the ith element of the third row (representing the vertical component) of the weighted geometry projection matrix used to generate the position estimate;

$\sigma_{i(j)}$ is the fault-free differential ranging error standard deviation for the i or jth satellite;

k_{md} is a missed detection multiplier (based on the prior probability of an ephemeris anomaly and the LAAS navigation integrity risk requirement allocated to ephemeris faults);

P_i is the ephemeris decorrelation parameter ("P-value") for satellite i. It is defined as the minimum detectable error (MDE) of the LGF ephemeris monitor divided by the antenna-SV range:

$$P_i = \frac{\text{MDE}}{\rho_i}. \quad (7)$$

The P-value is broadcasted by the LGF to airborne users for each satellite.

The relevant equation for LPLs under the ephemeris failure hypothesis is analogous; the only change is that the lateral components of the geometry projection matrix S are used in place of the vertical one.

In addition to VPL_e, the aircraft also computes a vertical protection level under the fault-free ($H0$) hypothesis. [1] To ensure navigation integrity, both protection levels, VPL_{H0} and VPL_e, are compared with a predefined position error bound known as the vertical alert limit (VAL). If ephemeris protection levels exceed the $H0$ protection levels computed by LAAS users ($\text{VPL}_e > \text{VPL}_{H0}$), LAAS availability will be reduced. From (6) and (7), it can be seen that the key factor to keep VPL_e small is to ensure that the LGF ephemeris monitor MDE is small.

Considering the most stringent case, VAL = 10 m at 200 ft altitude, LGF specifications [6] require that $P < 1.5 \times 10^{-4}$ to ensure adequate system availability. Conservatively taking the shortest possible range to a satellite from the Earth's surface (approximately 20,000 km), the resulting desirable MDE for the LGF ephemeris monitor is 3000 m. The remainder of this paper is dedicated to the direct validation of this fault detection requirement by defining the means to achieve it.

III. SENSITIVITY ANALYSIS

Prior to deriving specific fault detection algorithms, it is instructive to examine the general

TABLE I
GPS Satellite Ephemeris Parameters

Parameter	Definition
Δn	mean motion difference from Keplerian value
a	semimajor axis
e	eccentricity
i_o	inclination at t_{oe}
Ω_o (OMEGA$_0$)	longitude of ascending node of orbit plane at t_{oe}
ω	argument of perigee
M_o	mean anomaly at t_{oe}
t_{oe}	reference time for ephemeris
I_{dot} (IDOT)	rate of inclination angle
Ω_{dot} (OMEGADOT)	rate of right ascension
C_{is}, C_{us}	amplitudes of harmonic correction terms for
C_{rs}, C_{ic}	argument of latitude, orbit radius, and
C_{uc}, C_{rc}	angle of inclination
μ	Earth gravitational parameter (constant)
Ω_{Edot}	Earth rotation rate (constant)

TABLE II
GPS Orbit Model Formulas

Term	Formula
n_o	$(\mu/a^3)^{1/2}$
t_k	$t - t_{oe}$
n	$n_o + \Delta n$
M_k	$M_o + nt_k$
M_k	$E_k - e\sin(E_k)$
ν_k	$\tan^{-1}(\{[(1-e^2)^{1/2}]\sin(E_k)\}/[\cos(E_k)-e])$
ϕ_k	$\nu_k + \omega$
δu_k	$C_{us}\sin(2\phi_k) + C_{uc}\cos(2\phi_k)$
δr_k	$C_{rs}\sin(2\phi_k) + C_{rc}\cos(2\phi_k)$
δi_k	$C_{is}\sin(2\phi_k) + C_{ic}\cos(2\phi_k)$
r_k	$a[1 - e\cos(E_k)] + \delta r_k$
u_k	$\phi_k + \delta u_k$
i_k	$i_o + \delta i_k + i_{dot}t_k$
x'_k	$r_k\cos(u_k)$
y'_k	$r_k\sin(u_k)$
Ω_k	$\Omega_o + (\Omega_{dot} - \Omega_{Edot})t_k - \Omega_{Edot}t_{oe}$
X^*_k	$x'_k\cos(\Omega_k) + y'_k\cos(i_k)\sin(\Omega_k)$
Y^*_k	$x'_k\sin(\Omega_k) + y'_k\cos(i_k)\cos(\Omega_k)$
Z^*_k	$y'_k\sin(i_k)$

Note: Satellite positions in ECEF coordinates.

sensitivity of satellite position error to variations (i.e., potential errors) in the broadcast ephemeris parameters. Given the time-of-ephemeris (t_{oe}) and the fifteen broadcast GPS ephemeris parameters for a given satellite defined in Table I

$$[p_1,\ldots,p_{15}] = [a, M_0, \Delta n, e, \Omega_0, i_0, I_{dot}, \ldots] \tag{8}$$

we can compute the satellite position (x_{sv}, y_{sv}, z_{sv}) at any time t:

$$\begin{bmatrix} x_{sv}(t) \\ y_{sv}(t) \\ z_{sv}(t) \end{bmatrix} = \begin{bmatrix} f(p_1,\ldots,p_{15},t_{oe},t) \\ g(p_1,\ldots,p_{15},t_{oe},t) \\ h(p_1,\ldots,p_{15},t_{oe},t) \end{bmatrix} = \begin{bmatrix} f(p,t_{oe},t) \\ g(p,t_{oe},t) \\ h(p,t_{oe},t) \end{bmatrix} \tag{9}$$

where p is the 15-element parameter vector, and f, g, and h are nonlinear functions defined by the satellite position algorithms in GPS ICD-200C [7], which are repeated in Table II.

Now consider sensitivity to parameter variations:

$$\begin{bmatrix} \delta x_{sv}(t) \\ \delta y_{sv}(t) \\ \delta z_{sv}(t) \end{bmatrix} = \begin{bmatrix} \dfrac{\partial f(p,t_{oe},t)}{\partial p_1} & \cdots & \dfrac{\partial f(p,t_{oe},t)}{\partial p_{15}} \\ \dfrac{\partial g(p,t_{oe},t)}{\partial p_1} & \cdots & \dfrac{\partial g(p,t_{oe},t)}{\partial p_{15}} \\ \dfrac{\partial h(p,t_{oe},t)}{\partial p_1} & \cdots & \dfrac{\partial h(p,t_{oe},t)}{\partial p_{15}} \end{bmatrix} \begin{bmatrix} \delta p_1 \\ \vdots \\ \delta p_{15} \end{bmatrix}. \tag{10}$$

In a more compact form, we can write

$$\delta r(t) = A(p,t_{oe},t)\delta p \tag{11}$$

where A is the 3×15 sensitivity matrix which can be computed either analytically or numerically by partial differentiation of f, g, and h. The last equation is then a linearized expression directly relating parameter and position variation. Each term in the sensitivity matrix is a function of 15 reference broadcast parameters and is also an explicit function of time.

In parallel, a full year of ephemerides from all satellites was used to quantify the distribution of daily variations for each ephemeris parameter. The standard deviations of each of these parameter variation distributions were computed. As discussed shortly, daily (24 h) ephemeris variations are directly relevant to LAAS monitors that are based on the use of prior ephemeris data. Using the sensitivity matrix and the standard deviations of the daily parameter variations it is possible to determine 1 σ satellite position error variations due to nominal daily variations on the individual ephemeris parameters.

Fig. 1 shows position error sensitivity results for an example reference ephemeris parameter set. The t_{oe} of this ephemeris corresponds to the center of the x axis in the plot (12 h from an arbitrary 0 value). The 1 σ satellite position error contribution due to the 1 σ daily variation of each individual parameter is shown in the separate traces in the figure. The values computed and shown go from $t = t_{oe} - 12$ h, to $t = t_{oe} + 12$ h.

The individual 1 σ errors due to M_0 and ω variations are not directly plotted in the figure, because daily variations in these parameters are not independent, but rather exhibit a strong (almost perfect) negative correlation. This correlation is due to the fact that the GPS orbits are nearly circular, making it difficult to explicitly distinguish between M_0 and ω in the orbit determination process. With nearly circular orbits, the argument of latitude, $M_0 + \omega$ is more convenient to use because it is always well

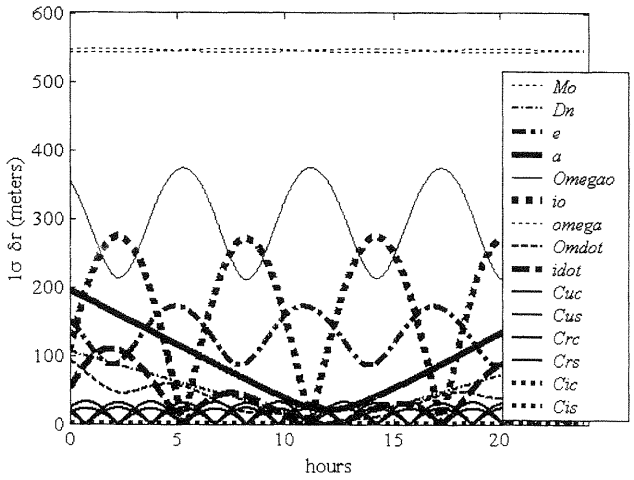

Fig. 1. Sensitivity of satellite position error to daily parameter variations.

defined, and any issues of correlation between these two parameters are avoided. In this regard, the traces for M_0 and ω shown in the figure were computed using the corresponding sensitivity associated with the individual parameters and the standard deviation of daily variations in argument of latitude. The result, the two uppermost traces in the figure, shows that satellite position error using previously validated ephemerides will be affected by variations in argument of latitude more than by any other parameter.

The curves corresponding to the two least influential parameters, C_{ic} and C_{is}, appear as nearly flat dashed lines at the bottom of the plot and never surpass the half-meter level. This last observation is advantageous with regard to postmaneuver monitoring as discussed in more detail later in this paper.

IV. DETECTION OF TYPE B ANOMALIES

As each new ephemeris is received it must be validated prior to use. In this section, we deal only with newly rising satellites. These satellites represent the worst case because the last validated ephemeris can be up to 24 h old. The results for the subsequent ephemeris changeovers (every 2 h) on the same day will be significantly better because nominal parameter variations will be much smaller. [3]

For a given current ephemeris and time epoch k (with k being the relative time with respect to t_{oe}: $k = t - t_{oe}$) we can compute the satellite position vector r_k. We can also compute the satellite position $\hat{r}_k$, for the same time using our best prior estimate of the current ephemeris based on previously validated ephemerides. The difference between the two will yield a position deviation vector $\delta r_k = r_k - \hat{r}_k$. Under nominal conditions (no ephemeris anomalies) δr_k data may be collected over many days to generate fault-free empirical distributions and covariance matrices $\Sigma_{\delta r_k}$. In the results that follow, an entire year of ephemeris data for all the satellites in the GPS constellation is used. Position errors (δr_k) and covariance matrix ($\Sigma_{\delta r_k}$) elements are expressed in local level coordinates (intrack, crosstrack, and radial).

Because parameter variations can affect the position errors differently with time relative to t_{oe}, the analysis was done for different value of k: -2 h, -1 h, and 0, to discretely cover the entire time of broadcast ephemeris validity. In general, the worst results (i.e., largest fault-free variation) were consistently at $t = t_{oe}$ ($k = 0$) [8], so these are the results mainly shown in this section.

Consider now a monitor that generates δr as discussed above. We now define a normalized scalar test statistic as follows:

$$s_k = \delta r_k^{\mathrm{T}} \Sigma_{\delta r_k}^{-1} \delta r_k. \tag{12}$$

The test statistic is compared with a threshold T to detect an anomalous ephemeris. The threshold is defined to ensure a fault-free alarm probability Pr(FFA) that is consistent with the system availability and continuity requirements. Prior analysis by Pullen [3] has shown that for rising satellites (whose ephemeris is yet to be validated) a FFA probability of 1.9×10^{-4} is sufficient for LAAS Category I. Under normal conditions, s will be approximately chi-square distributed with three degrees of freedom. The corresponding formula to find the threshold is then [9]:

$$\begin{aligned} \Pr(\mathrm{FFA}) = 1.9 \times 10^{-4} &= 1 - \int_0^T \frac{t^{(\nu-2)/2} e^{-t/2}}{2^{\nu/2}\Gamma(\nu/2)} dt \\ &= 1 - \frac{1}{\sqrt{2\pi}} \int_0^T t^{1/2} e^{-t/2} dt \end{aligned} \tag{13}$$

where ν is the number of degrees of freedom, and Γ is the Gamma function. In this case, we have a threshold $T = 4.4456^2$.

We next turn our attention to the derivation of the monitor MDE. It is shown by Shively in [10] that a missed detection (MD) probability of 10^{-3} is sufficient for the ephemeris integrity monitor. Given an ephemeris anomaly, the test statistic will have a nearly noncentral chi-square distribution. The minimum noncentrality parameter (λ) for such a distribution that is consistent with the required probability of MD Pr(MD), for the monitor is given by (14) [9]

$$\Pr(\mathrm{MD}) = 10^{-3} = \sum_{j=0}^{\infty} \frac{(\lambda/2)^j}{j!} e^{-\lambda/2} \Pr[\chi^2_{3+2j} \le T]. \tag{14}$$

In this case, $\lambda = 7.3618^2$.

A satellite position error δr_e will be detectable with the required MD probability if

$$\lambda \le \delta r_e^{\mathrm{T}} \Sigma_{\delta r_k}^{-1} \delta r_e. \tag{15}$$

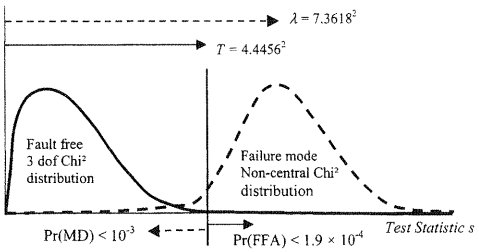

Fig. 2. Threshold and noncentrality parameter.

(See Fig. 2.) The vector δr_e of maximum length that fails to satisfy this inequality defines the MDE

$$\text{MDE} = \sqrt{\lambda q} \tag{16}$$

where q is the maximum eigenvalue of $\Sigma_{\delta r_k}$.

It is clear that small MDE values require that the covariance matrix $\Sigma_{\delta r_k}$ (or more precisely, its maximum eigenvalue) be small. A small covariance, in turn, can only be achieved by using an accurate satellite position estimator to generate $\hat{r}$. For the limiting case of a newly rising satellite, the most obvious choice is to use the last validated ephemeris of the prior day, which is always less than 24 h old. Projected satellite position estimates $\hat{r}_k$ can be generated directly from the prior ephemeris for comparison with the corresponding position r_k obtained from the current ephemeris-to-validate (E_{TV}). Alternatively, the 15-element parameter vector from the prior day can first be referenced to the t_{oe} corresponding to the E_{TV} by advancing the mean anomaly (M_0), inclination (i_0), and longitude of the ascending node (Ω_0) to the new reference time. (This adjustment is easily executed using the rates for these parameters, which are also available from the prior ephemeris.) Both approaches, generally referred to as "yesterday ephemeris minus today ephemeris" (YE-TE) methods, provide the same position estimate $\hat{r}_k$ at any given time. The latter method, however, being implemented via a parameter zero-order hold (ZOH), is more useful because it can be extended to more advanced parameter projection algorithms as discussed below.

Some parameter combinations—in particular argument of latitude, as noted earlier—vary considerably from day to day. [8] Therefore, it is advantageous to consider estimators based on two or more prior days of data. Toward this purpose, the behavior of ephemeris parameters with time was investigated. As a representative example, Fig. 3 shows the broadcast semi major axis (a) values for a particular SV over a 45-day interval. Fig. 4 shows values taken 24 h apart to filter short-period variations.

The natural daily variations in the parameters, unaccounted for in the ZOH, can be partially captured using a first-order hold (FOH). The FOH estimator uses a linear projection based on two prior days of data; it is distinguished from the ZOH as illustrated in Fig. 5.

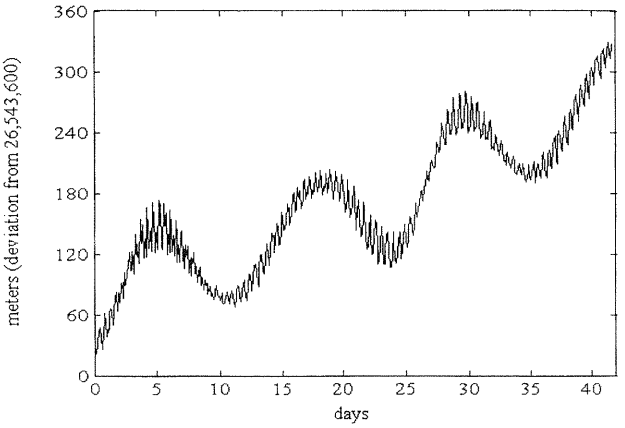

Fig. 3. Values of parameter a with time.

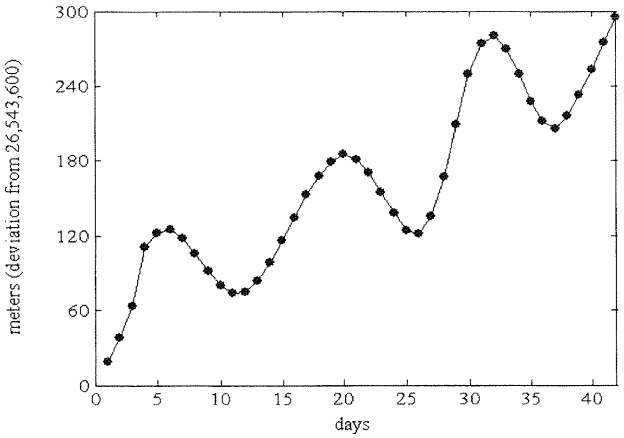

Fig. 4. Values of parameter a at 24 h intervals.

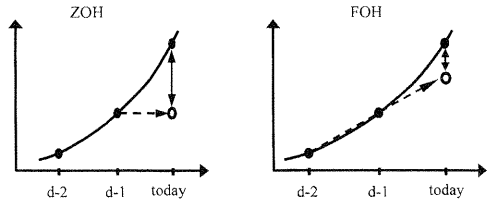

Fig. 5. Parameter estimation using ZOH and FOH.

The distribution of fault-free satellite position error $|\delta r_k| = |r_k - \hat{r}_k|$ using the two different parameter projection methods for a one year-span of ephemeris data (combining all satellites) is shown in Fig. 6. It is obvious from the results that the FOH estimator yields a much tighter distribution of fault-free error.

A second-order hold (SOH), using three prior days of data, was also investigated and shown to give even better results. For example, for the prediction of $M_o + \omega$, the fault-free estimate error standard deviation was 2.65×10^{-6} rad for the SOH, compared with 4.33×10^{-6} for the FOH and 1.16×10^{-5} for the ZOH. Nevertheless, it is demonstrated here that the FOH estimator performance is sufficient to meet

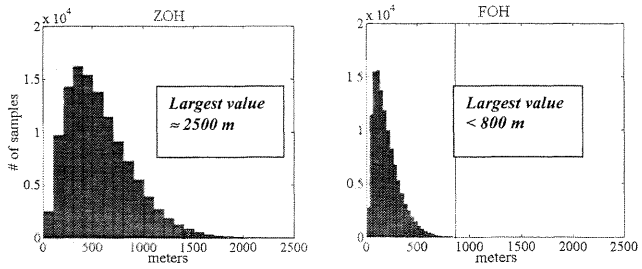

Fig. 6. ZOH and FOH position error (δr) distributions.

the MDE target of 3000 m. For this reason, and the fact that a SOH implementation would require an additional prior day of ephemeris data to validate E_{TV}, the SOH was not pursued further.

Based on the complete set of ephemerides for all satellites for the year 2002, Fig. 7 shows the distributions of test statistic s at t_{oe} ($k = 0$) for the ZOH and FOH monitors. For this data set, the allowable number of samples (N_s) whose values are larger than T is given by the product of the allowable FFA probability and the total number of samples (in this set 117,380):

$$N_s = \Pr(\text{FFA}) \times \text{Samples}$$
$$= 1.9 \times 10^{-4} \times 117{,}380 = 22.3 \approx 22. \quad (17)$$

In Fig. 7 it can be observed that the number of samples exceeding the detection threshold is bigger than N_s for both monitors (126 for the ZOH and 57 for the FOH). This is caused by the fact that the test statistic s is not perfectly chi-square distributed. To avoid this problem, the covariance matrices must be inflated to reduce the number of FFAs below N_s. The adjusted test statistic is

$$s_k = \delta r_k^{\mathrm{T}} (C\Sigma_{\delta r_k})^{-1} \delta r_k \quad (18)$$

where C is the necessary inflation factor. For the ZOH and FOH monitors using the year-span data set, the inflation factors are $C_{ZOH} = 1.36$ and $C_{FOH} = 1.19$.

To verify that the chi-square distribution is conservative for the adjusted test statistic, the cumulative distribution function (cdf) of the test statistic data was compared with the theoretical chi-square cdf. This comparison is shown in Fig. 8 for the ZOH case, from which it can be observed that

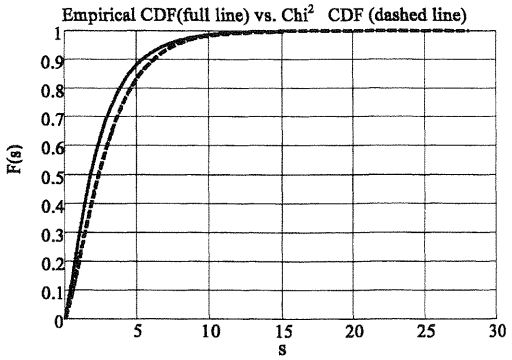

Fig. 8. CDF of test statistic s.

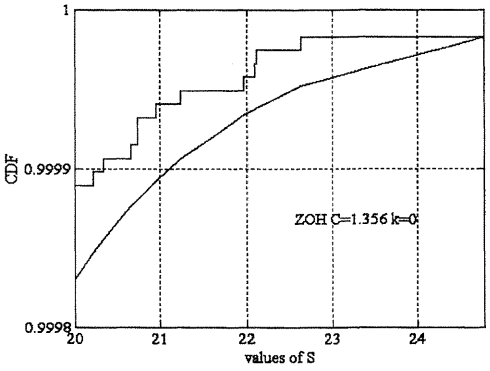

Fig. 9. Tail overbounding of cdf for ZOH.

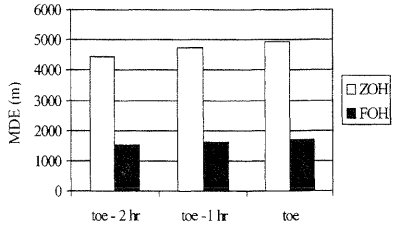

Fig. 10. MDEs for all satellites combined.

the lower theoretical cdf never surpasses the value of the upper empirical cdf. The cdf "tail" regions are expanded in Fig. 9. The FOH case was similarly verified.

It is possible now to compute the MDE using formula (16), by using the inflated covariance ($C\Sigma_{\delta r_k}$). The results, for three representative times during the E_{TV} period of validity (beginning, middle, and end) are shown in Fig. 10. The worst case, at t_{oe}

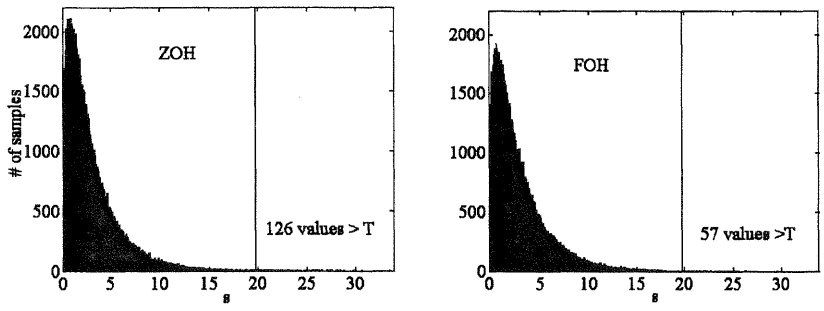

Fig. 7. Distribution of test statistic s.

TABLE III
Missed Detection Empirical Verification Results

Estimation Method	Total # of Erroneous Positions Generated	Errors > MDE	Magnitude of Maximum Undetected Error (MUX)	Undetected Errors > MDE	# Undetected Errors Between MUX and 2 × MDE − MUX
ZOH	5,634,420	1,117,901	5035 m	9	14/115,718
FOH	5,634,420	3,367,151	1763 m	2	7/41,442

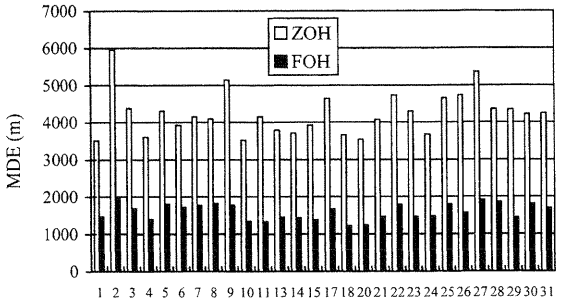

Fig. 11. MDEs for individual satellites.

($k = 0$) yields $\text{MDE}_{\text{ZOH}} = 4984$ m and $\text{MDE}_{\text{FOH}} = 1744$ m.

It is also important to understand that when the position error data is separated by satellite, significant variation in MDE exists for both the ZOH and FOH implementations. Fig. 11 shows the MDE results for individual satellites. (It is worth noting that the satellites with the largest MDEs typically have larger-than-average orbit eccentricity.)

Fault detection performance was also verified experimentally by deliberately injecting anomalous parameters in otherwise nominal ephemeris broadcasts. For all ephemerides in the 2002 year-span data, position coordinates (r) were generated first with the fault-free parameters (p), and then again after introducing (one parameter at a time) an error δp to cause errors in the satellite position of a magnitude similar to the derived MDE values. The relative time k was 0 in all cases. The true position error (Δr) caused by the deliberately introduced parameter error was then computed:

$$\Delta r = r - r_{\text{faulty}} = r(p) - r(p, p_i + \delta p_i). \tag{19}$$

An estimated position error was also computed:

$$\Delta \hat{r} = \hat{r} - r_{\text{faulty}} = r(\hat{p}) - r(p, p_i + \delta p_i) \tag{20}$$

with $\hat{p}$ representing either the ZOH or FOH parameter estimates, depending on which of the two estimators was used. By introducing $\Delta \hat{r}$ in place of δr in (18), and comparing the resulting value of s with the threshold T, it is determined whether or not the failure was detected.

Table III shows that the results of this empirical analysis agree with the analytically derived MDE values. For the ZOH, the largest undetected error was 5035 m, 51 m larger than the MDE value. To get a more complete idea of the MD probability at the MDE value borderline, the bin with values between MDE − 51 m and MDE + 51 m was considered in more detail. The total number of undetected errors is listed in the last column of the table along with the number of total position errors in that bin. Only 14 out of 115,718 position errors were not detected.

Similar analysis was performed for the FOH. In this case, the maximum undetected error being 1763 m, 19 m above the MDE. In the bin between MDE − 19 m and MDE + 19 m, 7 out of 41,442 errors were not detected. For both the ZOH and FOH estimators, the percentage is significantly below the 10^{-3} MD constraint.

It is clear from Figs. 10 and 11, that the FOH is sufficient to ensure LAAS availability (MDE < 3000 m), whereas the ZOH is not (MDE > 3000 m). The principle drawback of the FOH is that it requires two prior days of ephemerides, in contrast to the ZOH, which needs only one. However this is not a significant liability because two prior days are always available at the LGF, except after a station-keeping maneuver. Such maneuvers happen about once per year per satellite. In this case, on the second day following a maneuver, the FOH implementation cannot be used since only one prior day's worth of ephemeris is available. A related issue of general concern is how to validate the broadcast ephemeris on the day immediately following a satellite maneuver. In this case, there is no prior (useful) ephemeris data available. This subject is discussed in the next section. However, it is worth noting at the outset that this issue is also relevant to the implicit assumption in any YE-TE implementation that prior ephemeris data is fault free; whereas in reality, the prior days' orbit was only validated to be consistent with a specified MDE.

V. DETECTION OF TYPE A1 ANOMALIES

After a scheduled maneuver, the orbit parameters change significantly, making previous ephemerides useless for validation via YE-TE. In this event, a potential solution is to verify the postmaneuver broadcast ephemeris directly by the use of LGF code and carrier phase measurements. To determine whether or not such an approach is effective and realizable, we assume that we have one day available immediately following the maneuver (during which

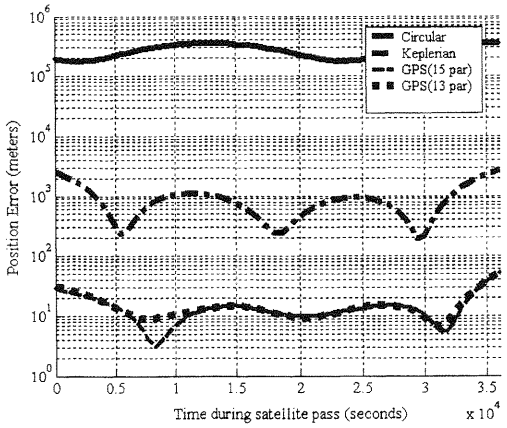

Fig. 12. Residual position errors for different orbit models.

corrections are not broadcasted) to verify the current ephemeris. Once verified, this ephemeris may be used on the following day in a YE-TE-type monitor implementation. Such a procedure can also be used on a daily basis to confirm the fault-free assumption on the prior day's ephemeris used in YE-TE.

The basic idea behind this monitor implementation is to fit the collected LGF measurements to an orbit model to obtain a source of satellite position that is independent of the broadcast ephemeris. The selection of a proper orbit model is based on a tradeoff between model complexity and fault-free accuracy of the model. In this regard, Fig. 12 illustrates the fault-free satellite position error for an example satellite using three simple orbit models: circular, Keplerian, and the GPS orbit model. (The last one refers to the standard 15 parameter GPS ephemeris model.) In each case, fault-free satellite position data for an entire satellite pass was fit via least squares to the candidate models, and the residual position errors (model-fit minus true position) were generated.

The results show that the circular and Keplerian models are not accurate enough for our purposes because the residual model errors alone are much larger than the MDE we must achieve (for the circular model) or nearly equal to them (for the Keplerian case). In contrast, using only one set of GPS model parameters for the whole satellite pass gives maximum errors smaller than 60 m. This is adequate for our purposes. An additional GPS orbit model, eliminating parameters C_{is} and C_{ic}, was also evaluated. These parameters have a negligible impact on the satellite position error (as shown previously in Fig. 1). The reduced GPS model is simpler in structure and ultimately provides better orbit estimation results because fewer parameters need to be estimated from the limited data that is available. As can be seen in Fig. 12, this model is also sufficiently accurate for our needs.

At least two measurements available within the LGF are potentially useful for orbit estimation. These are the stand-alone pseudo-range residual (i.e., the broadcast pseudo-range correction) and the differential carrier phase across the LGF reference receiver baselines. The measurement models are described below

The stand-alone pseudo-range residual measures the orbit error over time (k) projected into the satellite's LOS direction e_k:

$$z_k^\rho = e_k^{\mathrm{T}} \delta r_k + v_k^\rho \tag{21}$$

where the measurement error is distributed as $v_k^\rho \sim N(0, \sigma_\rho^2)$. Since this is a nondifferential measurement, the error will be highly correlated over time due to the effect of the ionosphere. Time correlation of these measurements must be taken into account in the orbit estimation process.

The differential carrier residual measures orbit errors orthogonal to the LOS and projected into a known baseline direction. In this analysis we assume two orthogonal baselines of equal length. For each baseline, the measurement equation is

$$z_k^\phi = \ell \frac{d^{\mathrm{T}} E_k}{\rho_k} \delta r_k + \Delta\tau_k + N\lambda + v_k^\phi \tag{22}$$

where ℓ is the baseline length, d is the baseline direction unit vector, $E_k \equiv I - e_k e_k^{\mathrm{T}}$, I is the 3×3 identity matrix, $\Delta\tau_k$ is the clock offset between receivers, N is the carrier integer cycle ambiguity, λ is the L1 carrier wavelength (19.04 cm), and v_k^ϕ is the measurement error due to receiver thermal noise and multipath. In this case, the measurement error is also time correlated, but over much shorter time scales. Sampling over 4 min intervals effectively whitens these measurements. The receiver clock offset is easily removed by differencing against a nominal satellite that has not been maneuvered and has passed all recent monitor tests. This term is not considered further in the analysis.

The initial state vector includes the ephemeris parameters, and the two cycle ambiguities (one for each baseline). Covariance analysis results have shown that with measurement data available for a whole satellite pass, the standard deviation of the error in the cycle ambiguity estimates is significantly lower than 10^{-2} carrier wavelengths. Therefore, the cycle ambiguities can be rounded to the nearest integer with a negligible probability of error. In the analysis that follows, the cycle ambiguities are assumed to be resolved and removed from the differential carrier phase measurement, making $N = 0$ in (22).

Substituting (11) into measurements (21) and (22), we obtain measurement equations in terms of the orbit parameter error vector (δp) rather than the time-varying satellite position error vector (δr_k):

$$z_k^\phi = \frac{\ell}{\rho_k} d^{\mathrm{T}} E_k A_k \delta p + v_k^\phi \Rightarrow z_k^\phi = H_k^\phi \delta p + v_k^\phi. \tag{23}$$

Stacking measurements collected over a day (for baselines a and b), we have

$$\begin{bmatrix} z_1^\rho \\ \vdots \\ z_n^\rho \\ \hline z_{a1}^\phi \\ \vdots \\ z_{an}^\phi \\ z_{b1}^\phi \\ \vdots \\ z_{bn}^\phi \end{bmatrix} = \begin{bmatrix} H_1^\rho \\ \vdots \\ H_n^\rho \\ \hline H_{a1}^\phi \\ \vdots \\ H_{an}^\phi \\ H_{b1}^\phi \\ \vdots \\ H_{bn}^\phi \end{bmatrix} \delta p + \begin{bmatrix} \upsilon_1^\rho \\ \vdots \\ \upsilon_n^\rho \\ \hline \upsilon_{a1}^\phi \\ \vdots \\ \upsilon_{an}^\phi \\ \upsilon_{b1}^\phi \\ \vdots \\ \upsilon_{bn}^\phi \end{bmatrix} \Rightarrow z = H\delta p + \upsilon. \tag{24}$$

The measurement error is distributed as $\upsilon \sim N(0,V)$ where

$$V = \left[\begin{array}{c|c} V^\rho & 0 \\ \hline 0 & I\sigma_\phi^2 \end{array}\right] \tag{25}$$

and σ_ϕ is the standard deviation of the differential carrier phase measurement error. The size of the identity matrix in (25) is $2n \times 2n$. The submatrix V^ρ accounts for the time correlation of pseudo-range measurements and is defined for any element (i,j) using an exponential model:

$$V_{ij}^\rho = \sigma_\rho^2 \exp(|i-j|\Delta t/\tau). \tag{26}$$

In (26), Δt is the measurement sample interval and τ is the time constant of the pseudo-range measurement error. As noted earlier, we choose Δt = 4 minutes so that differential carrier measurements are decorrelated. Due to the ionosphere, however, stand-alone pseudo-range measurements are correlated over much longer times. In this work we use τ = 12 h, but covariance analysis in [8] showed that the overall MDE results are not particularly sensitive to the specific value used, as long at it is on the order of the length of a typical satellite pass (i.e., much larger than Δt). The value of differential carrier error standard deviation is chosen in this analysis to be consistent with LAAS integrated multipath limiting antenna (IMLA) performance: σ_ϕ = 0.3 cm. Stand-alone pseudo-range error standard deviation is dominated by ionospheric error and set conservatively in this analysis at σ_ρ = 10 m.

The weighted least squares solution to (24) is

$$\delta\hat{p} = (H^{\mathrm{T}}V^{-1}H)^{-1}H^{\mathrm{T}}V^{-1}z \tag{27}$$

and the associated parameter estimate error covariance matrix is

$$\Sigma_{\delta p} = (H^{\mathrm{T}}V^{-1}H)^{-1}. \tag{28}$$

Recall that the satellite position error is related to the parameter error by (11): $\delta r_k = A_k \delta p$. The position error covariance at any time epoch k is then

$$\Sigma_{\delta r_k} = A_k \Sigma_{\delta p} A_k^{\mathrm{T}} \tag{29}$$

which may be substituted directly into (16) to obtain a comparable MDE for each given time relative to t_{oe}. The MDE traces for all satellites in the constellation are shown in Fig. 13 for a Chicago O'Hare LGF site. For each SV, t is arbitrarily set to zero in the figure at that given satellite's rise time. The magnitude of the MDE for each satellite is directly related to the geometric diversity and length of the pass. The worst case (upper) curves in the plot all have short passes. In contrast, satellites that are visible during two different time segments on the same day (connected by straight lines in the figure) have the lowest MDE values. Different markers distinguish results for different baseline lengths in the figure.

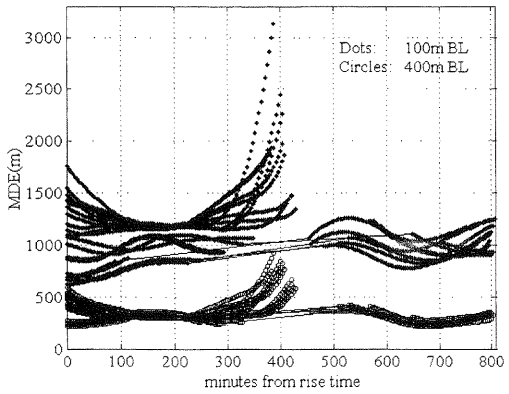

Fig. 13. MDE versus time for all satellites.

It is evident from the results in the figure that MDEs below 3000 (our desired target) are generally achievable for baseline lengths of 100 m. It is also clear that the MDE is dramatically improved as the baseline length is increased. Because the MDE results will also be sensitive to the LGF location, a baseline of 200 or 400 m may be required depending on the particular LGF location. Determining the necessary distance between the antennas that form the baselines is very important as the airports have physical constraints regarding their siting.

In addition, achieving MDEs smaller than the YE-TE MDEs in Section III is desirable to support the YE-TE monitor assumption that the prior days' ephemerides are fault free. In this regard, the algorithm described in this section can be implemented to postprocess data every day to ensure that the YE-TE assumptions are true. A rough quantitative measure of the impact on the total MDE can be seen in Table IV. The approximate total MDE was computed using relation (30) by combining the $\mathrm{MDE}_{\mathrm{meas}}$ from the measurement-based monitor (taking maximum values from Fig. 13) with the $\mathrm{MDE}_{\mathrm{FOH}}$

TABLE IV
Total MDE Values for Different Baseline Lengths

Baseline Length	MDE_{meas}	MDE_{FOH}	Total MDE
100 m	3137 m	1744 m	4767 m
200 m	1743 m	1744 m	3020 m

derived for the FOH in Section IV

$$MDE \approx \sqrt{2 \times MDE_{meas}^2 + MDE_{FOH}^2}. \quad (30)$$

The coefficient 2 on MDE_{meas} accounts for the fact that with the FOH monitor, two independent prior days of ephemeris data must be validated using the measurement-based technique. The MDE_{FOH} term accounts for the independent error associated with the FOH projection of fault-free prior ephemerides. The preliminary results in the table suggest that for baseline lengths as short as 200 m the impact on availability would likely be minimal (recall the desired MDE value is 3000 m). Rigorous validation of these results and experimental verification of the measurement based monitor is in progress and will be published in a future paper.

VI. CONCLUSIONS

Algorithms to monitor broadcast ephemerides for Category I Local Area Augmentation of GPS are proposed. It is shown that the use of an FOH ephemeris parameter estimator is sufficient to detect type B orbit ephemeris anomalies with MDEs well below 3000 m, which is sufficient to meet LAAS specifications. A simpler ZOH approach is shown insufficient in this regard. It is also shown by means of covariance analysis that type A1 ephemeris anomalies can be detected through the direct use of available (single-frequency) LAAS measurements. The achievable MDE using this approach is a strong function of baseline length, but it is shown that baseline lengths between 100 and 400 m are generally sufficient to meet the navigation system requirements (with substantial margin at the upper end of this baseline range). The relevance of the measurement-based monitor to the confirmation of type B monitor assumptions is also discussed.

ACKNOWLEDGMENTS

The constructive comments and advice regarding this work provided by Samer Khanafseh and Samuel P. Pullen are greatly appreciated.

REFERENCES

[1] Minimum Operational Performance Standards for GPS Local Area Augmentation System Airborne Equipment. RTCA SC-159 WG-4A, DO-253, Washington, D.C., Jan. 11, 2000.

[2] Pervan, B., and Chan, F-C. Detecting global positioning satellite orbit errors using short-baseline carrier phase measurements. *Journal of Guidance, Control, and Dynamics*, **26**, 1 (Jan.–Feb. 2003).

[3] Pullen, S., Lee, J., Luo, M., Pervan, B. Chan, F-C., and Gratton, L. Ephemeris protection level equations and monitor algorithms for GBAS. In *Proceedings of the 14th International Technical Meeting of the Satellite Division of the Institute of Navigation*, Salt Lake City, UT, Sept. 11–14, 2001.

[4] Zumberge, J., and Bertiger, W. Ephemeris and clock navigation message accuracy. *Global Positioning System: Theory and Applications*, (Progress in Aeronautics and Astonautics, Vol. 163), New York: AIAA, 1996.

[5] Chan, F-C. Detection of global positionin system orbit errors using short baseline carrier phase measurements. M.S. thesis, Dept. of Mechanical, Materials, and Aerospace Engineering, Illinois Institute of Technology, Chicago, Aug. 2001.

[6] Specification: Category One Local Area Augmentation System Non-Federal Ground Facility. United States Department of Transportation, Federal Aviation Administration, FAA/AND710-2937, May 31, 2001.

[7] Interface Control Document (ICD) GPS-200, Revision B Rockwell International, 1987.

[8] Gratton, L. Orbit ephemeris monitors for category I local area augmentation of GPS. M.S. thesis, Dept. of Mechanical, Materials, and Aerospace Engineering, Illinois Institute of Technology, Chicago, July 2003.

[9] Abramowitz, M., and Stegun, A. *Handbook of Mathematical Functions*. New York: Dover, 1972.

[10] Shively, C. LAAS integrity risk due to satellite ephemeris faults. In *Proceedings of the 14th International Technical Meeting of the Satellite Division of the Institute of Navigation*, Salt Lake City, UT, Sept. 11–14, 2001.

Boris Pervan received a B.S. from the University of Notre Dame, Notre Dame, IN (1986), M.S from the California Institute of Technology, Pasadena (1987), and Ph.D. from Stanford University, Stanford, CA (1996), all in aerospace engineering.

From 1987 to 1990, he was a systems engineer at Hughes Space and Communications Group involved in spacecraft mission analysis for both commercial and government programs. He was a research associate at Stanford from 1996 to 1998, serving as project leader for GPS Local Area Augmentation System (LAAS) research and development. He is now assistant professor of Mechanical and Aerospace Engineering at the Illinois Institute of Technology (IIT) in Chicago.

Dr. Pervan received the 1996 RTCA William E. Jackson Award. He was also the 1999 recipient of the M. Barry Carlton Award from the IEEE Aerospace and Electronic Systems Society, the 2002 Ralph Barnett Award for excellence in teaching at IIT, the Abert J. Zahm Prize in Aeronautics at Notre Dame (1986), and the Guggenheim Fellowship at Caltech (1987). He is a council member of the Institute of Navigation (ION) and an associate editor of the ION journal *Navigation*.

Livio Gratton received a Mechanical Engineering Degree from the Escuela Superior Técnica del Ejército in Buenos Aires, Argentina, in 2000. In 2003 he received his M.S. degree in aerospace engineering at the Illinois Institute of Technology, Chicago. He is a Ph.D. candidate in the same university, and is currently working in failure monitoring for DGPS-based approach and landing.